# Transport, Heat, and Freshwater Fluxes within a Diagnostic Numerical Model (FRAM)

P. M. SAUNDERS AND S. R. THOMPSON

*Institute of Oceanographic Sciences, Godalming, Surrey, United Kingdom*

(Manuscript received 4 June 1991, in final form 16 April 1992)

ABSTRACT

Results are presented from the integration of a fine-resolution numerical model of the ocean operating in a diagnostic mode. The region covered lies south of 24°S, as depicted in the FRAM Atlas. Here transports, heat, salt, and freshwater fluxes are examined at 60°S and near 30°S in all three oceans. Results are found to be generally realistic.

At midlatitude the meridional heat flux is largely determined by the structure of the mean meridional motions and to a lesser degree by the gyre-scale horizontal motions. These roles are reversed for freshwater fluxes. At a fixed high latitude the freshwater flux is determined by the mean meridional motions and the heat flux principally by the large-scale wandering of the circumpolar current across the latitude. Only in this latter case, namely for the heat flux at 60°S, do mesoscale motions contribute to a significant extent.

The model underestimates the production and export of abyssal water; the climatological state with which it is initialized is identified as the likely cause. A suggestion is offered for assessing the accuracy of diagnostic integrations.

## 1. Introduction

The numerical ocean model, Fine Resolution Antarctic Model (FRAM), was set up primarily to investigate momentum and vorticity balances within the Southern Ocean (Webb et al. 1991a). A robust diagnostic scheme was used to initialize the model, and, after approaching an equilibrium state, FRAM was run as a prognostic model. In this second phase, climatologies have been constructed and the model dynamics has been studied. Results will be reported elsewhere.

The diagnostic state preceded the prognostic. It was simpler in that, with the exception of the wind stress, surface boundary fluxes (including rainfall) were not represented. At high latitudes this task is particularly taxing because the formation, advection, and melting of ice must be described.

This paper presents results from FRAM in the diagnostic phase and primarily at just one time step. We wish to draw the attention of oceangoing scientists to these results as representing the state of the art of current numerical ocean models. Many observationalists have spent a lifetime measuring the distribution of temperature, salinity, and chemical tracers in the ocean and have then employed simple dynamical procedures to infer the circulation. The diagnostic phase of FRAM is a very complex and objective way of doing the same. Thus, we suppose the results will be of interest to oceangoers.

The authors had no control over the development of the FRAM project, so we were unable to explore the dependence of the results on the numerous parameters, approximations, and boundary conditions that it was necessary to assume. Nevertheless, by examination of the internal consistency of the results and by our knowledge of, and by comparison with, the ocean we have been able to establish both strengths and weaknesses of the model. These strengths and weaknesses will, for the most part, be carried forward into the prognostic phase of the integration, which modelers consider to be the most important aspect of their research.

Thus, the authors look to two groups of readers: observationalists to inform them of and entrain their interest in state-of-the-art ocean modeling, and modelers to assist them in recognizing and, hence, rectifying weaknesses in their numerical models. Many perceive a gulf in communication between these two groups; if this is true we wish to help bridge it.

## 2. The diagnostic phase

Table 1 summarizes the characteristics of the FRAM; see Webb et al. (1991a).

The distinguishing feature of the integration in the diagnostic phase is inclusion in the thermodynamic equations of a term that forces the model everywhere to a prescribed condition. For this condition, the climatic state of the ocean, as represented by the analysis

*Corresponding author address:* Dr. Peter M. Saunders, Institute of Oceanographic Sciences, Brook Road, Wormley, Godalming, Surrey, GU8 5UB, United Kingdom.

TABLE 1. The characteristics of FRAM.

| | |
|---|---|
| Origin | Cox (1984) Primitive equations, finite difference on a sphere |
| Grid-size | 1/2° in longitude, 1/4° in latitude |
| Levels | 32, spacing 20–230 m (Table 2) |
| Viscosity | $2 \times 10^2$ m$^2$ s$^{-1}$ and $10^{-4}$ m$^2$ s$^{-1}$ |
| Diffusivity | $10^2$ m$^2$ s$^{-1}$ and $.5 \times 10^{-4}$ m$^2$ s$^1$ |
| Domain | between 24°S and 79°S |
| Area | $1.23 \times 10^{14}$ m$^2$ (One-third of World Ocean) |
| Bathymetry | based on DBDB5, smoothed to 1° (Killworth 1987) |
| Northern boundary condition | interior flow Sverdrup: boundary current to conserve transport (Stevens 1990) |
| Surface stress | Hellerman and Rosenstein (1983), annual mean for diagnostic phase |
| Initial state | $S = 36.69$, $\theta = -2$°C at rest |
| Final state | forced to be near Levitus (1982), velocity diagnosed |

of Levitus (1982), was selected. Because of the very high resolution and extent of FRAM it was the obvious candidate. The equations for both salinity $S$ and potential temperature $\theta$ are taken to be of the form:

$$\text{storage} + \text{advection} = \text{diffusion} + \text{relaxation},$$

with the relaxation term, which was introduced by Sarmiento and Bryan (1982), in the form $1/\tau$ (Levitus—model). During the integration $\tau$ was varied, but for the last 3.5 years had a value of one year. Had a larger value of $\tau$ been selected, the integration would have required longer in order to converge. A smaller value would have damped out the mesoscale motions; the succeeding prognostic integration would have become convulsively unstable, and the approach to steady state would also have required a longer integration. The value chosen was believed to be an optimum compromise. In the interval of five to six years, the total kinetic energy of the model became approximately constant, so that at the end of the period the integration was terminated (Webb et al. 1991a).

The six-year analysis has been published in atlas form (Webb et al. 1991b), showing the property and velocity fields on horizontal surfaces along with vertical sections on the paths defined by World Ocean Circulation Experiment (WOCE) core 1 and core 2 projects (WOCE 1988). These illustrations should be thought of as companions to this paper and none will be reproduced here. An examination of the atlas reveals that the property distributions possess considerable mesoscale eddy structure and frontal features, which are not present in the smooth initial data; see the plates on pp. 12, 20, and 31. The structure is time dependent, appears realistic, and is testimony to the weakness of the relaxation term in the thermodynamic equations. The representation of the $\theta$, $S$, and velocity fields at six years is available publicly in digital form (de Cuevas 1990).

What significance should be attached to these results? Let us define a true prognostic integration of FRAM as one in which the relaxation term is removed and the model ocean is forced by only boundary fluxes. Such an integration if carried to an equilibrium state would require about two orders of magnitude more resources than were available to the FRAM project, to judge by the experience of Bryan (1987). Suppose, in such a conceptual experiment, a model climatology was constructed of the equilibrium state. A diagnostic version of the integration could then be carried out, forced by the model climatology. Only in such circumstances, we argue, would it be possible to evaluate the performance of a diagnostic integration such as this paper reports.

Some readers might consider that this consideration disqualifies the diagnostic integration from meriting serious study. We believe otherwise. The case for the diagnostic integration rests on three arguments. First, we do what we can! Second, the results of the diagnostic phase are generally quite similar to those imperfect versions of the prognostic integrations of FRAM, all of which exhibit climatic drift (Thompson, personal communication). Third, the results from the diagnostic integration appear realistic, as will be demonstrated in the following sections. Nevertheless, it is clear that an evaluation of the method, widely used in one form or another, would be helpful even if employed on a coarse resolution model with simplified topography.

## 3. The approach to thermodynamic equilibrium

Because of another researcher's work on the momentum and vorticity balance of FRAM (Stevens 1992), the primary, but not exclusive, emphasis in this paper will be on the fluxes of mass, heat, and salt. First it is necessary to consider the closeness of the thermodynamic variables to a truly equilibrium state.

The overall mean salinity and potential temperature of the Levitus data within the FRAM region are 34.67 and 2.80°C. [The salinity was measured prior to introduction of the practical salinity scale (psu), and temperature prior to the introduction of ITS-90: the distinctions will be ignored throughout this paper.] The FRAM model ocean, everywhere initially at 36.69 and −2.0°C, remains after six years of integration 0.011 more saline and 0.011°C cooler.

The equilibrium state will be defined here as one in which the storage or rate of change integrated over the entire FRAM volume vanishes. This state is not actually reached, however. Between years 5 and 6 of the model integration the storage term for potential temperature, that is, heat, falls from about 4.1 PW (1 PW = $10^{15}$ W) to 1.5 PW (Fig. 1a), while the relaxation term falls from 3.2 PW to 0.7 PW. The difference, representing the advective and diffusive flux through the open (northern) boundary of FRAM, decreases from 0.9 PW to 0.8 PW, a very slight change indeed. The decay appears to be exponential and this is confirmed by fitting such a function. The rate of decay has a time

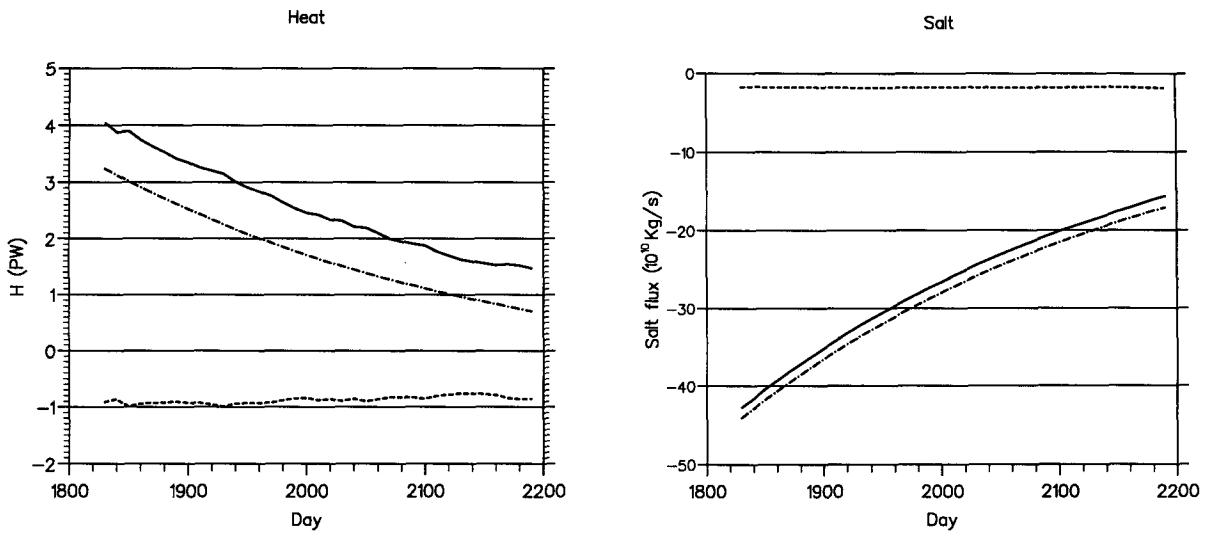


FIG. 1. The approach to equilibrium for the model integration period 5–6 years: (a) potential temperature (heat). Upper curve: storage, middle: relaxation, lower: boundary flux. (b) As in (a) but for salinity (fresh water). Upper curve: boundary flux, middle: storage, lower: relaxation.

constant of 360 ± 10 days for both the storage and relaxation terms, as we might expect if the other terms in the equation were small. Thus, had the integration of the model proceeded for two more model years the heat storage term would have been less than 0.1 PW and, together with the relaxation term −0.7 PW and boundary flux 0.75 PW, would have balanced to zero.

The salt balance equation exhibits a similar behavior (Fig. 1b), with the storage and relaxation terms decaying exponentially, the former to zero and the latter to a value of about $-1.8 \times 10^{10}$ kg s$^{-1}$, which sums with the boundary flux to zero. The exponential decay rate has a time constant of 360 ± 10 days. Note that as with the heat flux, the boundary flux at equilibrium is close to the value after six years of integration.

Thus, the equilibrium state of FRAM in the diagnostic phase is predicted to have a southward heat flux of 0.75 PW at the northern boundary. Since there is no heat flux either across any solid boundary within the model or across the upper surface, this southward heat flux is removed by a heat sink represented by the relaxation term. The heat sink has no physical significance, of course, but has a counterpart in reality: we shall suppose that the divergence of the heat flux that results is a virtual representation of the exchange across the surface. Support for this view is found by noting that the relaxation term is largest in the upper 50 m, is moderate from there to 400 m, and virtually vanishes in the depth range 1500–4500 m (the difference between the FRAM equilibrium temperature and Levitus exceeds 0.5°C, 0.1°C but does not exceed 0.005°C, respectively, in these three layers). Overall, in FRAM the meridional heat flux decreases with increasing southerly latitude and this we take to represent the net loss of heat to the atmosphere (see Carissimo et al. 1985). Such a conclusion is inescapable if one supposes that the heat fluxes in FRAM are realistic.

In the equilibrium state a southward flux of salt of about $1.8 \times 10^{10}$ kg s$^{-1}$ is predicted at the northern boundary. It too is removed by a sink represented by the relaxation term. Fluxes of salt within FRAM were unexpected, for one might suppose that in a steady state salt flux must be zero. Over the real ocean, precipitation exceeds evaporation in most middle to high latitudes but elsewhere, outside of a narrow equatorial belt, the reverse is true. The meridional motions of the atmosphere carry the water between these latitudes and, consequently, the ocean must maintain the balance. Thus, in the real ocean the mass flux, say across a zonal section, is not quite zero. In FRAM by virtue of its code (Cox 1984) the two roles are reversed; the mass flux is zero, but the salt flux is not.

The salt flux in FRAM should thus be interpreted as a virtual mass flux. Consider the northern boundary. If a mass flux of 18/35 or 0.5 Sv (1 Sv ≡ $10^6$ m$^3$ s$^{-1}$) were allowed to escape northward, which would require a mean motion of only $0.5 \times 10^{-6}$ cm s$^{-1}$, the salt flux would then be zero (in such a calculation the mean salinity of the section needs to be known but a value of 35 is usually sufficiently accurate). Stommel (1980) and others have termed this the freshwater flux carried by the ocean, but it is rather the negative of the freshwater flux carried by the atmosphere! Thus, the 0.5 Sv of virtual mass transported northward in FRAM estimates the impact on the ocean of rainy mid–high latitudes and dry low latitudes. As will be mentioned later, the estimate is realistic. Note also that the virtual mass fluxes are sufficiently small that they can be ignored in discussing the transports within the ocean, which are measured in tens or hundreds of Sv.

## 4. The treatment of the six-year output and definitions

Along a prescribed, zonal track, $\theta$, $S$, eastward $u$ and northward $v$ components of the velocity were extracted at the 32 model levels together with the latitudes and longitudes. For each ocean basin and each latitude the output was placed in a separate file and treated as if it were a line of CTD stations, thus making available software in routine use. Because the property output ($\theta$, $S$) and the velocity output ($u$, $v$) are staggered by half-grid spacing with respect to each other, first the property components were averaged from the locations immediately north and south of the velocity line. The pair average thus falls at the midpoints of the velocity locations. For heat and salt flux calculations, values of neighboring velocity locations must then be averaged onto the location of the property output. This treatment is consistent with the internal operation of the model.

In the calculations that follow, the output so derived has been further treated in the following way. Let an overbar represent the section average at a fixed level, namely:

$$\bar{v}(j) = \frac{1}{n} \sum_{i=1}^{n} v(i, j),$$

where $v$ is the meridional component of velocity (northward positive) at location $i$ (or station number $i$, $i = 1$ to $n$) and depth or level $j$, $j = 1, 32$. The deviation $v'(i, j) = v(i, j) - \bar{v}(j)$ represents the deviation from the horizontal average for the $n$ locations at level $j$.

The contribution to the volume flux $M$ from the level $j$ is

$$dM(j) = \sum_{i=1}^{n} v(i, j) \cdot \Delta x \Delta z = n\bar{v}(j)\Delta x \Delta z(j),$$

since $\Delta x$ the station separation, for fixed latitude, is constant and $\Delta z(j)$ the layer depth is constant. The layer depth for each level is shown in Table 2. The units used are Sv $\equiv 10^6$ m$^3$ s$^{-1}$. The total volume flux across a circumpolar section or across a zonal section extending from coast to coast is zero, namely:

$$M = \sum_{j=1}^{32} dM(j) \equiv 0.$$

The heat flux is calculated from the product $v\theta$, namely, the contribution to the heat flux from the level $j$ is $dH = \sum_{i=1}^{n} v(i, j)\theta(i, j)\Delta x \Delta z(j)$. A similar expression is employed for the salt flux. The total heat flux across the section is $H = \sum_{j=1}^{32} dH(j)$. It is convenient to use the units Sv °C, which are converted to petawatts by dividing by 233.

By virtue of the resolution above, the heat flux contribution may also be written:

TABLE 2. FRAM levels and layers.

| Level | Thickness (m) | Middepth (m) |
|---|---|---|
| 1 | 20.7 | 10. |
| 2 | 23.3 | 32. |
| 3 | 26.5 | 57. |
| 4 | 31.0 | 86. |
| 5 | 37.3 | 120. |
| 6 | 46.7 | 162. |
| 7 | 61.6 | 216. |
| 8 | 85.9 | 290. |
| 9 | 121.0 | 393. |
| 10 | 156.0 | 532. |
| 11 | 180.0 | 700. |
| 12 | 195.0 | 887. |
| 13 | 205.0 | 1087. |
| 14 | 211.0 | 1295. |
| 15 | 215.0 | 1508. |
| 16 | 219.0 | 1725. |
| 17 | 221.0 | 1945. |
| 18 | 223.0 | 2167. |
| 19 | 225.0 | 2391. |
| 20 | 226.0 | 2617. |
| 21 | 227.0 | 2843. |
| 22 | 228.0 | 3071. |
| 23 | 229.0 | 3299. |
| 24 | 230.0 | 3529. |
| 25 | 230.0 | 3759. |
| 26 | 231.0 | 3989. |
| 27 | 231.0 | 4220. |
| 28 | 232.0 | 4452. |
| 29 | 232.0 | 4684. |
| 30 | 233.0 | 4916. |
| 31 | 233.0 | 5149. |
| 32 | 233.0 | 5382. |

$$dH(j) = \sum_{i=1}^{n} \bar{v}(j)\bar{\theta}(j)\Delta x \Delta z(j) + \sum_{i=1}^{n} v'(i, j)\theta'(i, j)\Delta x \Delta z(j),$$

where the first term represents the contribution to the heat flux carried by the section-averaged motion and the second represents the contribution carried by the deviation from the section average. Numerical modelers sometimes describe the second term as the eddy contribution, but this practice is misleading since the deviation term contains contributions from *all* scales and may be either quasi steady or transient. Here the term eddy will only be used in the conventional oceanographic sense, namely, to describe transient mesoscale processes.

## 5. Vertically integrated transports within FRAM

The six-year output was selected from two latitudes, a high latitude at 60°S, and a middle latitude at 30°S (Table 3). This choice allowed us to examine the three major oceans of the Southern Hemisphere as well as the Circumpolar Ocean.

TABLE 3. Characteristics of zonal sections studied.

| Designation | Ocean | Latitude, S | Number of stations | Spacing (km) | Longitude span | |
|---|---|---|---|---|---|---|
| | | | Low latitude | | | |
| A10 | Atlantic | 32.5 | 143 | 47 | 52.5°W | 18.5°E |
| I5 | Indian | 30 | 169 | 48 | 30.5°E | 114.5°E |
| P6 | Pacific | 30 | 271 | 48 | 153.5°E | 71.5°W |
| | | | High latitude | | | |
| S4 | Circumpolar | 60 | 720 | 28 | 0°E | 0°W |

The strength of the Antarctic Circumpolar Ocean (ACC), as manifest by the total transport through Drake Passage, is 195 Sv (Webb et al. 1991a). The commonly accepted observed value is 130 Sv (Whitworth et al. 1982), and the difference may arise because of inadequacies in the model physics, or because the Hellerman and Rosenstein wind stress (1983) is an overestimate (Chelton et al. 1990), or because (and this seems less likely) the observational data has failed to capture all of the transport. Which among these explanations is correct is, we believe, yet to be proven.

Although this paper does not set out to address the question of what determines the strength of the ACC, two observations will be made here.

Johnson and Bryden (1989) proposed that the easterly momentum imparted by surface wind stress was transported downward to the ocean floor by a mechanism involving mesoscale transient motions, or eddies. As a consequence the Ekman transport in the ACC would vanish. In FRAM this process is not at work. The Ekman layer at 60°S exists (Fig. 2 right) and has precisely the magnitude expected of the wind stress.

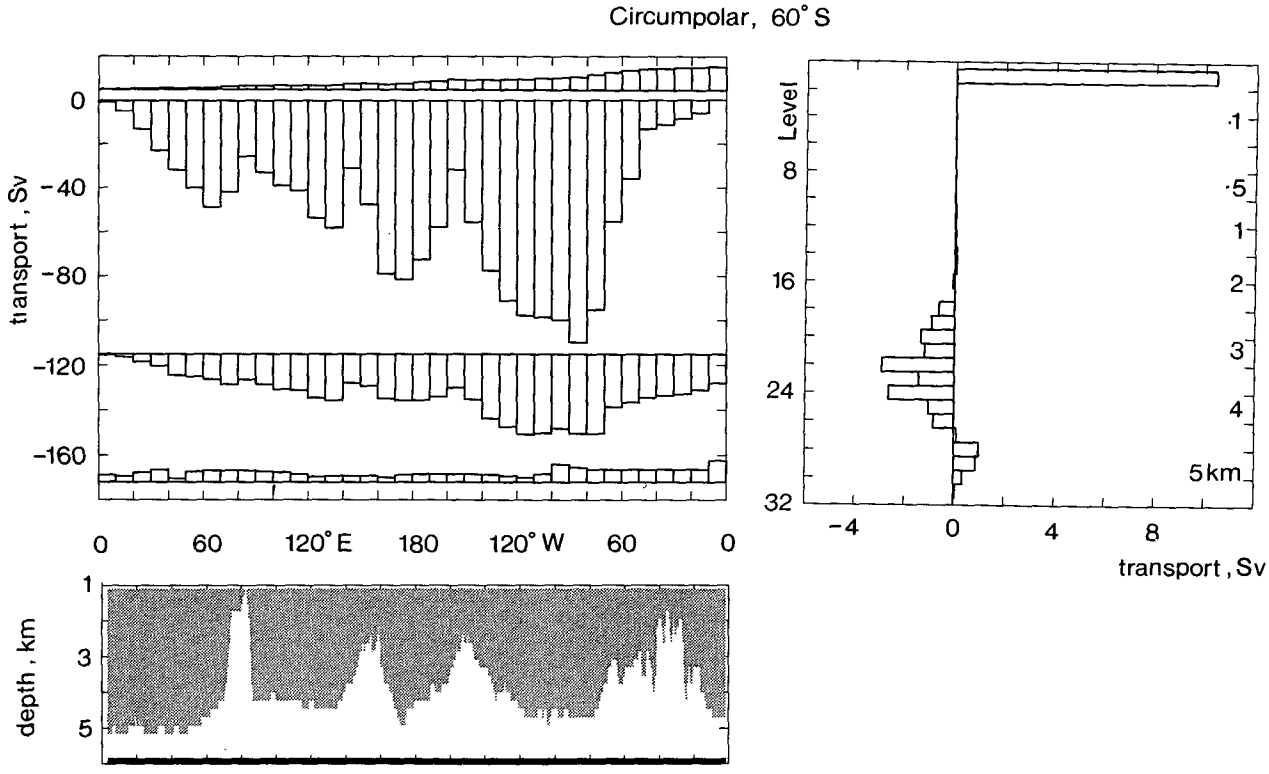


FIG. 2. Transport at 60°S. Bottom left, bathymetry. Top right, the mean meridional circulation showing the transport contribution (in Sv) by each level. North is +ive and the overall level sum is zero. Top left, the transport in the layers 0–20 m, 20–2000 m, 2000–4100 m, and >4100 m. The transport is accumulated from the Greenwich meridian in 5° longitude intervals and emphasizes the large-scale flow. At the right margin the net layer flow reflects the values found in the figure to its right.

TABLE 4. Transports in Sv in the major current systems.

| | Latitude (deg) | Depth range (m) | Transport | |
|---|---|---|---|---|
| | | | FRAM 6-yr | Wind stress |
| Brazil Current | 32.5 | 0–2500 | −27[a] | −32 |
| Agulhas Current | 30 | 0–3500 | −65 | −50 |
| E. Australia Current | 30 | 0–3400 | −38 | −47.5 |

[a] Considerable difficulty is experienced in separating the subtropical gyre from the export of North Atlantic Deep Water.

However, a return flow at depth must be set up, and if it is geostrophic then the pressure force required to balance the Coriolis term has a magnitude equal to the surface stress (see the Appendix).

If momentum balance is essentially assured by mass conservation, one must appeal to the vorticity balance to understand the strength of the ACC. The curl of the wind stress at 60°S is such that alone it would balance a southward planetary advection of −153 Sv. This is very close to that observed in FRAM [see Fig. 2 (left)]. The northward transport of +153 Sv required to bring about zero net transport across the section invokes the action of planetary advection, lateral friction, and bottom pressure torques (Holland 1973). The exact manner in which the balance occurs is still under investigation, but it appears that the strength of the ACC is determined in much the same way as for midlatitude gyres. This result was anticipated by Stommel (1957).

The vorticity balance in the subtropical gyres appears simpler. From the FRAM results, the Brazil Current at 32.5°S in the Atlantic has a transport of 27 Sv, the Agulhas Current at 30°S in the Indian Ocean has a value of 65 Sv, and the East Australia Current at 30°S in the Pacific has a transport of 38 Sv. These values are close to the Sverdrup transports, determined from the curl of the annual mean wind stress to be 32, 50, and 47.5 Sv, respectively (see Table 4), and suggest that only in the Indian Ocean can the bottom-pressure torque term augment the strength of the boundary currents.

The return flow in the interior of these gyres is remarkably uniform (see the upper left panels of Figs. 3, 4, and 5). However, there is a weak increase in the northward currents near the eastern margin in the Atlantic and Pacific oceans revealing the presence of the Benguela (12 Sv) and Humboldt (5 Sv) currents, respectively.

## 6. The thermohaline transports

By integrating the poleward flow at fixed depth, the strength of the overturning or thermohaline circulation is revealed. Because the vertical diffusivity in FRAM

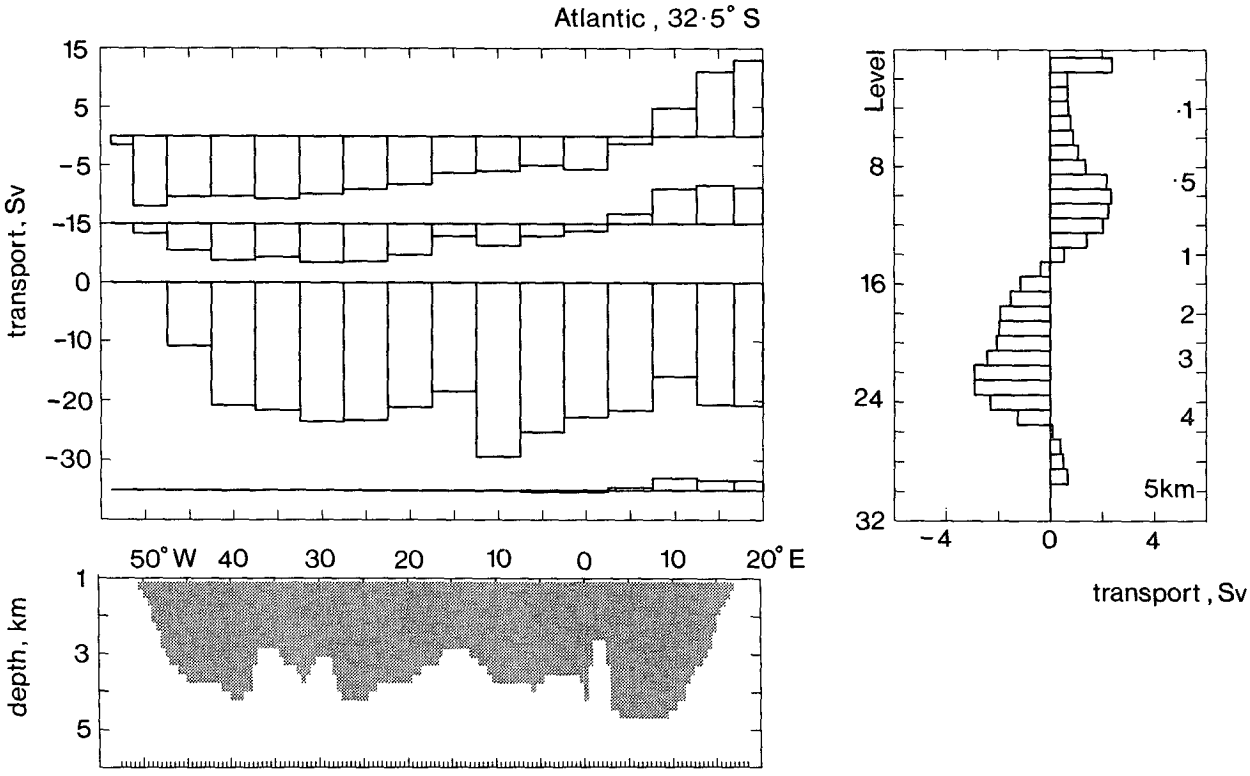


FIG. 3. Transport at 32.5°S in the Atlantic. As for Fig. 2 but note the layers in the top left figure are 0–700 m, 700–1500 m, 1500–3900 m, >3900 m. Now the transport is accumulated starting from the western boundary of the basin.

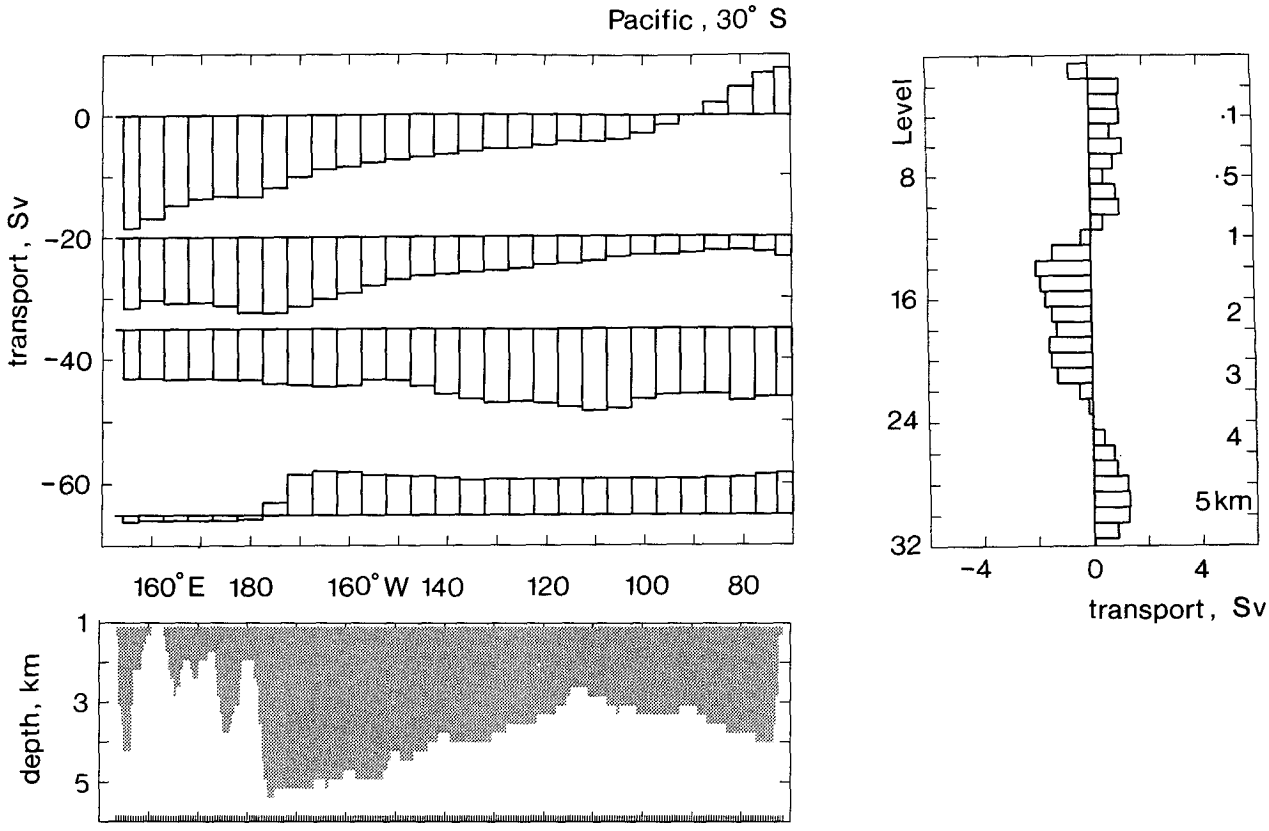


FIG. 4. Transport at 30°S in the Pacific. As for Fig. 3, but note the layers in the top left figure are 0–700 m, 700–1500 m, 1500–3400 m, >3400 m.

is small, 0.5 $cm^2\ s^{-1}$, the Ekman transport is confined to the upper layer, 0–20 m. Elsewhere, the flow is essentially geostrophic and by mass conservation its net strength must balance the Ekman value. Figures 2–5 (right panels) show its vertical distribution at 32 levels and Table 5 summarizes the results for four layers; surface, intermediate, deep, and abyssal.

The absence of a mean meridional flow in the layer 20–2000 m of the Circumpolar Ocean reflects the absence of topography at these depths, which is needed to support the geostrophic flow; elsewhere in all four oceans an overturning mode is found, which is strikingly diverse.

Consider first the Circumpolar Ocean where the major submarine ridges permit a southward flow of deep water above 4100 m and a northward flow at deeper levels. The export of bottom water has a magnitude of only 2.5 Sv, which many will consider derisory. Warren (personal communication) has estimated the true outflow as 18 Sv made up in the following way: −8 Sv from the Weddell Sea, 5 Sv from the Ross Sea (Gill 1973), and 5 Sv from sources distributed around the Antarctic continent.

A similar underestimate for the northward flow of abyssal water is found at 30°S in both the Atlantic and Pacific oceans. But in the Indian Ocean at this latitude the northward transport of both deep and bottom water (15.5 Sv) is close to the estimate of 19 Sv by Warren (1981) on 18°S.

In the Pacific, according to FRAM, the inflow of the abyssal water below 3400 m is only 7 Sv and is confined to a zone of 10° width east of the Kermadec–Tonga Ridge at 180° longitude (Fig. 4). This value is only about one-half of the inflow estimate of 12 Sv by Wunsch et al. (1983) and one-third of the 20 Sv estimated by Warren (1973). In the Atlantic there is no northward abyssal flow in the Argentine Basin (Fig. 3), whereas 4 Sv is expected near 40°W according to the observations of Hogg et al. (1982). Examination of the sections P6 in the Pacific and A9, A10 in the Atlantic (in the FRAM atlas) reveals that although cold bottom water is present on all these sections, it is not piled up steeply against the topography; it lacks the baroclinic structure, which is a striking feature of individual cruise data. In Fig. 6, a comparison is made for the two Atlantic sections to illustrate this point.

The absence of baroclinic structure at depth in the Levitus dataset appears endemic. The interpolation and averaging procedure used to create the climatology fails to represent isopycnal slopes adequately near boundaries, because of poor or sparse measurements, or for both reasons. Thus, the cause for the absence of suf-

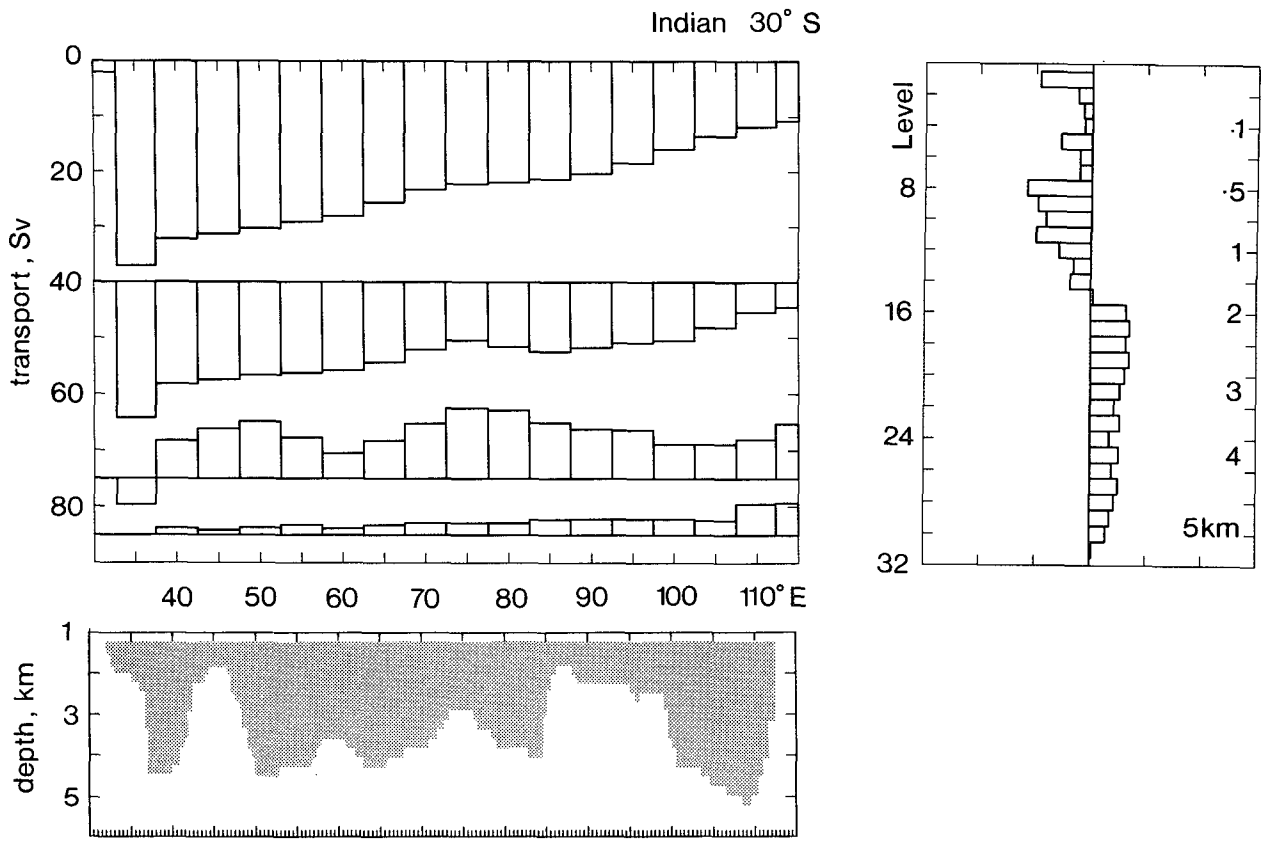


FIG. 5. Transport at 30°S in the Indian Ocean. As for Fig. 3, but note the layers in the top left figure are 0–700 m, 700–1500 m, 1500–3500 m, >3500 m.

ficiently strong abyssal flows in the FRAM six-year output resides outside the model. A second difficulty exists for the bottom flow on A10. The abyssal flow passes through the Vema Channel, a narrow 20-km-wide cleft in the topography with an actual sill depth of 4620 m that is represented in the smoothed FRAM bathymetry at a depth of 3700 m. Similar in-filling of the channels connecting the deep basins occurs throughout FRAM and this too must weaken the bottom flow.

This serious underestimate of the abyssal circulation is not apparently shared for shallower layers. Overall, the strength and direction of the overturning mode agrees reasonably well with the results of Rintoul (1988) for the Atlantic, with the results of Warren (1981) for the Indian Ocean, and with those of Wunsch et al. (1983) for the Pacific. These transports and their directions, coupled with estimates of the vertically integrated flow of the previous section, bestow an air of verisimilitude on the FRAM six-year output.

## 7. Oceanic heat fluxes in FRAM

The heat flux has been calculated as described in an earlier section across each of the four sections with the

TABLE 5. Net meridional transports in Sv (+ive northwards) in four layers.[a]

| | Circumpolar 60°S | Atlantic 32.5°C | Indian 30°S | Pacific 30°S |
|---|---|---|---|---|
| Surface | 10.5 | 13 | −11 | 8 |
| | 20 | 700 | 700 | 800 |
| Intermediate | 0 | 6 | −4.5 | −4 |
| | 2000 | 1500 | 1500 | 1500 |
| Deep | −13 | −20.5 | 10 | −11 |
| | 4100 | 3900 | 3600 | 3400 |
| Abyssal | 2.5 | 1.5 | 5.5 | 7 |

[a] Layer boundaries are given in meters with surface 0 and bottom 5500 m values omitted.

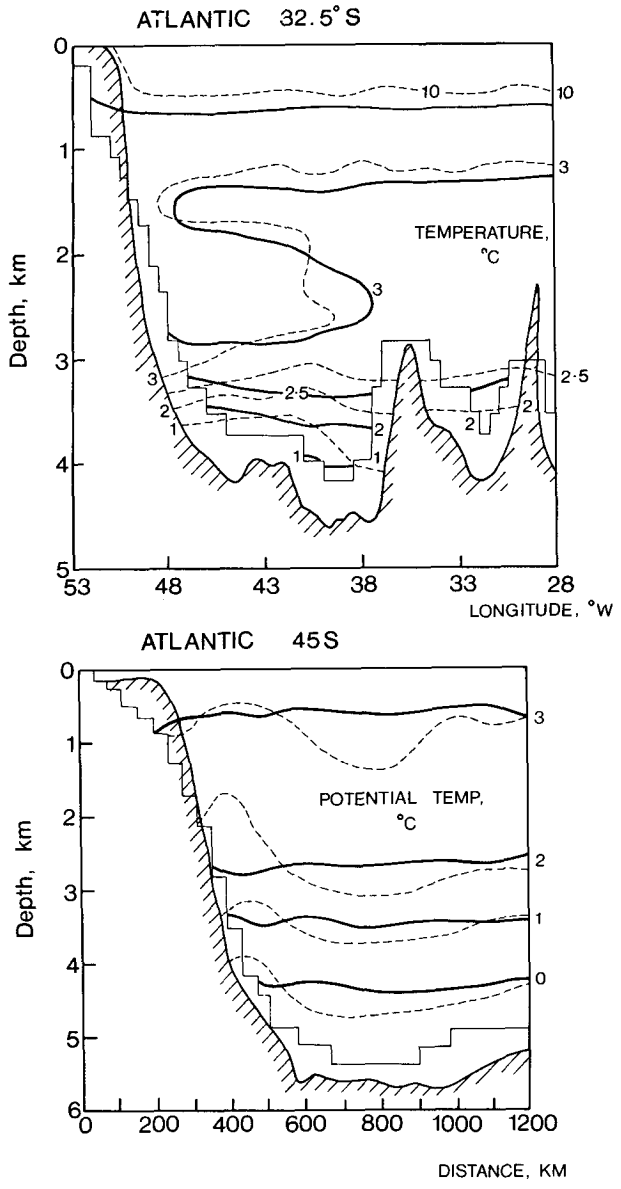


FIG. 6. Contours of (potential) temperature from the FRAM 6-year dataset inscribed on top of contours from observed sections. Upper figure, 32.5°S in the Atlantic, observations reported by Fuglister (1960). Lower figure, 45°S in the Atlantic, observations reported by Peterson and Whitworth (1989).

results displayed in Table 6. The contribution to the heat flux is divided into three parts: initially a split is made into the horizontal average and the deviation from it. The first term measures the mean meridional or thermohaline contribution and includes the Ekman flow; the second, the deviation from the horizontal mean, measures the impact of gyre and mesoscale processes. A separation of scales has been introduced by applying a running mean filter of width 13 grid points or 6.5° longitude to $\theta$, $S$, and $v$ variables to distinguish the contribution of large-scale and mesoscale processes. The total heat flux is given in units of both petawatts and Sv °C. The latter (unorthodox) unit is the more readily appreciated; a gyre of strength 30 Sv with a temperature contrast of 2°C contributes a heat flux of 60 Sv °C or 60/233 = 0.26 PW.

Consider first the heat flux components near 30° latitude. The contribution from the mean meridional motions is always large, being positive (northward) in both the Atlantic and Pacific and negative (southward) in the Indian Ocean. This merely reflects the direction of the (warm) upper-layer flow, northward in both former oceans (Figs. 3, 4) and southward in the latter (Fig. 5). Its magnitude is large because of the large vertical temperature gradient in the water column. The contribution from the essentially horizontal motions is always negative (southward) and dominated by the gyre-scale contributions. The gyres carry heat south because the western boundary currents are warmer than the returning interior flow. The contribution from the mesoscale is always small and, except in the Pacific, downgradient. (The prognostic version of FRAM shows an enhanced mesoscale activity but their contribution to the fluxes is still not as important as the other two processes.) Bryden and Hall (1980), in a seminal paper, found that at 25°N in the real ocean (North Atlantic) mesoscale processes were relatively unimportant agents of heat transfer.

Thus, the heat flux near 30°S is northward in the Atlantic where the contribution from the mean meridional overturning opposes but exceeds the gyre contribution, is zero in the Pacific where the two terms balance, and is southward in the Indian Ocean where the two terms augment each other. The magnitudes are quite similar to the estimates of Rintoul (1988), Wunsch et al. (1983), and Toole and Raymer (1985).

At 60°S the large-scale contribution to the heat flux is the dominant term; see Table 6. The thermohaline contribution is nil essentially because the vertical temperature gradient is very small, and mesoscale processes produce one-third of the transfer. Such a result is at variance with the widely held view that mesoscale eddies transport most, if not all, of the heat at high latitudes [for example, see Bryden (1979) and De Szoeke and Levine (1981)]. However, given the observed latitudinal excursions of the ACC, it is no surprise that the large-scale contribution to the heat flux is important and these have never been estimated in the real ocean.

To emphasize this result, the northward component of velocity $v$ has been combined with $\theta$ from the six-year output to yield the autospectrum of $v$ and the cospectrum $v\theta$, which are presented in Fig. 7 in variance-preserving form. The wavenumber scale $k$ spans the range from $k^{-1}$ = 20 000 km to $k^{-1}$ = 55 km. The energy in the mesoscale peaks at log$k$ = −2.5 ($k^{-1}$ = 325 km) but the cospectrum (heat), although showing the mesoscale contribution, is dominated by the very largest wavenumber. Such a figure is representative of levels 2–16 (20–1800 m), which are essentially un-

TABLE 6. FRAM heat fluxes on selected sections.

| Location | Latitude (°S) | Contribution to heat flux (Sv °C) | | | | Total PW |
|---|---|---|---|---|---|---|
| | | Total | Mean meridional | Deviation | | |
| | | | | Large scale | Mesoscale | |
| Atlantic | 32.5 | 130 | 166 | −32 | −4 | 0.56 |
| Pacific | 30 | 2 | 91 | −95 | 2 | 0.01 |
| Indian | 30 | −256 | −173 | −76 | −7 | −1.10 |
| Total | 30 | −126 | — | — | — | −0.53 |
| Circumpolar | 60 | −47 | 0 | −31 | −16 | −0.20 |

interrupted by topography, and which account for the bulk of the meridional heat transfer.

## 8. Oceanic salt (freshwater) fluxes in FRAM

The salt flux has been calculated in an identical manner to the heat flux: the units of Table 7 are $10^9$ kg $s^{-1}$ and contain the practical salinity units (psu), which are dimensionless. Here the conversion $10^9$ kg $s^{-1}$ = 1 Sv may be employed (some authors define ocean salinity $\equiv 35 \times 10^{-3}$, so their flux units are $10^6$ kg $s^{-1}$; the distinction should be readily apparent, however).

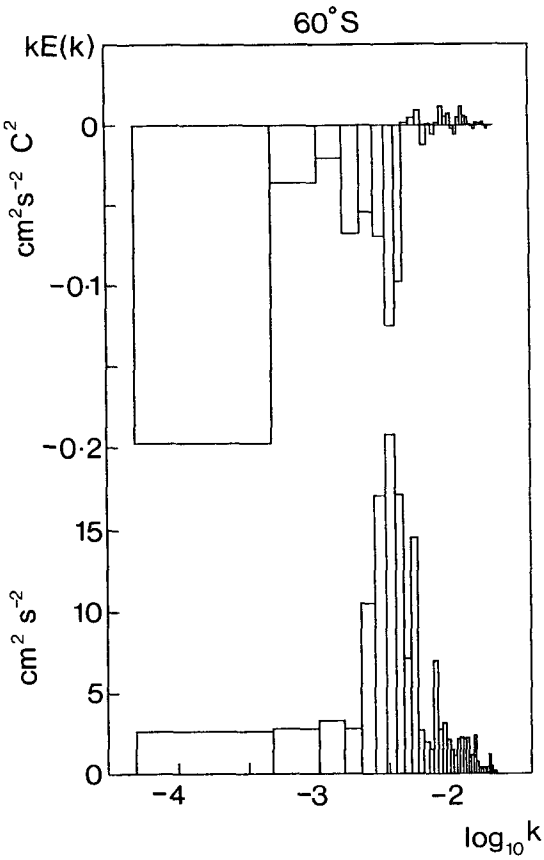


FIG. 7. Lower figure: the autospectrum of the north component of velocity at 30 m in variance-preserving form. The ordinate is $kE(k)$ and the abscissa is log$k$ where $k$ the wavenumber is $km^{-1}$. Upper figure: the cospectrum of the north component of velocity with the potential temperature—the contribution to the heat flux from the layer 20–40 m.

In all four ocean sections the salt flux is southward and the mesoscale contribution is again small. At 30°S the contribution from the thermohaline circulation is in the same direction as the flow in the upper layer, namely northward in the Atlantic and Pacific and southward in the Indian Ocean. In all of these oceans the gyre-scale contribution is southward because of the presence of saline water in the western boundary currents (see the FRAM Atlas) and overwhelms the northward overturning flux where it exists, and augments it where it is southward. The total southward salt flux, larger in the Indian and Pacific oceans than in the Atlantic, is a reflection of net northward transport of mass in the ocean and supplies the excess evaporation of low latitudes from the excess rainfall of mid to high. The FRAM estimates of these fluxes agree in sign with the results of Toole and Raymer (1985) for the Indian Ocean and Wunsch et al. (1983) for the Pacific but are somewhat larger.

In the Circumpolar Ocean the salt flux is again southward but is dominated by the contribution from the overturning motions: here fresh water in the Ekman layer with mean salinity 34.0 is replaced at depth by water of salinity 34.7. The Antarctic is correctly and commonly thought of as a source of the densest water in the world's oceans. Its role in providing large quantities of light, fresh cold water is easily overlooked.

## 9. Flux divergence south of 30°S

The heat and salt fluxes for the three major oceans are summed for the latitude 30°S (see Tables 6 and 7). The summation has the effect of neutralizing the impact of the flow between the Pacific and Indian basins, the Indonesian throughflow, which is ignored in FRAM. A heat flux of 0.54 PW southward is found, along with a northward freshwater flux of 0.64 Sv. Both have the expected sign.

If methods of estimating the heat flux carried by the ocean are reviewed, the conclusion is readily reached

TABLE 7. FRAM salt (freshwater) fluxes on selected sections.

| Location | Latitude (°S) | Contribution to salt flux ($10^9$ kg $s^{-1}$)[a] | | | | Freshwater flux (Sv) Total |
|---|---|---|---|---|---|---|
| | | Total | Mean meridional | Deviation | | |
| | | | | Large scale | Mesoscale | |
| Atlantic | 32.5 | −3.8 | 2.7 | −7.0 | 0.5 | 0.11 |
| Pacific | 30 | −9.0 | 4.6 | −13.1 | −0.5 | 0.26 |
| Indian | 30 | −9.5 | −6.0 | −4.5 | 1.0 | 0.27 |
| Total | 30 | −22.3 | — | — | — | 0.64 |
| Circumpolar | 60 | −6.4 | −7.1 | −0.1 | 0.8 | 0.19 |

[a] Nominal density of 1000 kg $m^{-3}$ has been assumed; the flux contains the dimensionless units of salinity.

that there is little possibility of deriving acceptably accurate results by appealing to meteorology. For example, a bias of only 10 W $m^{-2}$ in the estimates of surface exchange between ocean and atmosphere over the area covered by FRAM leads to an error in heat flux of 1.2 PW. This is larger than the meridional heat flux across the northern boundary of FRAM. If, as an alternative approach, the earth's radiation balance is examined, then low-latitude errors in meridional heat fluxes are found of precisely similar magnitude (Carissimo et al. 1985). So, we have not sought to pursue comparisons among the different methods at this time.

To emphasize the role played in the Southern Ocean by the Circumpolar Current, zonal heat and salt fluxes have been calculated at three locations. The results are listed in Table 8, and the locations shown in Fig. 8. Although the mass transport on the three sections is identical considerable variation is found in the meridional flux. Note in particular the relatively small heat transport found at 20°E, which is attributable to the net westward flow of heat carried by the Agulhas Current and its retroflection.

It should be noted that the heat fluxes (strictly enthalpy fluxes) are arbitrary: here the enthalpy flux is defined with respect to the enthalpy flux at 0°C. Similarly, there is arbitrariness about the zonal freshwater fluxes (see footnote to Table 8). However, there is no arbitrariness about the heat and freshwater flux divergences within the regions shown.

In the Pacific sector of the Southern Ocean (lower left), heat converges into the region and fresh water diverges from it. In other words, heat is lost to the atmosphere and fresh water gained, that is, there is excess rainfall. The Atlantic sector (upper left) exhibits a similar behavior. In the Indian Ocean sector (right) the Circumpolar Ocean south of 30°S gains heat from the atmosphere and loses fresh water to it, that is, there is excess evaporation. Of course, only the net exchanges within those regions are derived. High air–sea fluxes of improbable sign are not implied, but nevertheless the result is unexpected.

These results are quite different from those reported earlier by Stommel (1980) both in magnitude and sign. In the Pacific at 30°S, Stommel reported southward fluxes of both heat and fresh water, showing by an ingenious argument that the latter must have the wrong sign. He also concluded that the freshwater fluxes were generally exaggerated; the FRAM results appear more realistic. Indeed, the total northward freshwater flux across 30°S of 0.64 Sv found in FRAM is quite close to the meteorologically derived value of Bryan and Oort (1984). Woods (1985) presented oceanic heat fluxes derived in part from Stommel and also from Bryden. The FRAM results, especially on meridional sections, differ strikingly from both these estimates and are often substantially larger. The differences are in part explained by the large transport (195 Sv) in the FRAM circumpolar current.

TABLE 8. Zonal heat, salt, and freshwater fluxes in the Circumpolar Ocean.

| Location | Longitude | Heat flux | | Salt flux ($10^9$ kg $s^{-1}$) | Freshwater flux[a] (Sv) |
|---|---|---|---|---|---|
| | | (Sv °C) | PW | | |
| Drake Passage | 60°W | 409 | 1.83 | 6724.4 | 0.17 |
| S. Africa | 20°E | 237 | 1.08 | 6714.4 | 0.46 |
| Tasmania | 147°E | 540 | 2.42 | 6730.4 | 0 |

[a] Zonal freshwater flux has an arbitrary zero; here the salt flux on the Tasmanian section is first subtracted before dividing by the mean salinity (circa 34.5).

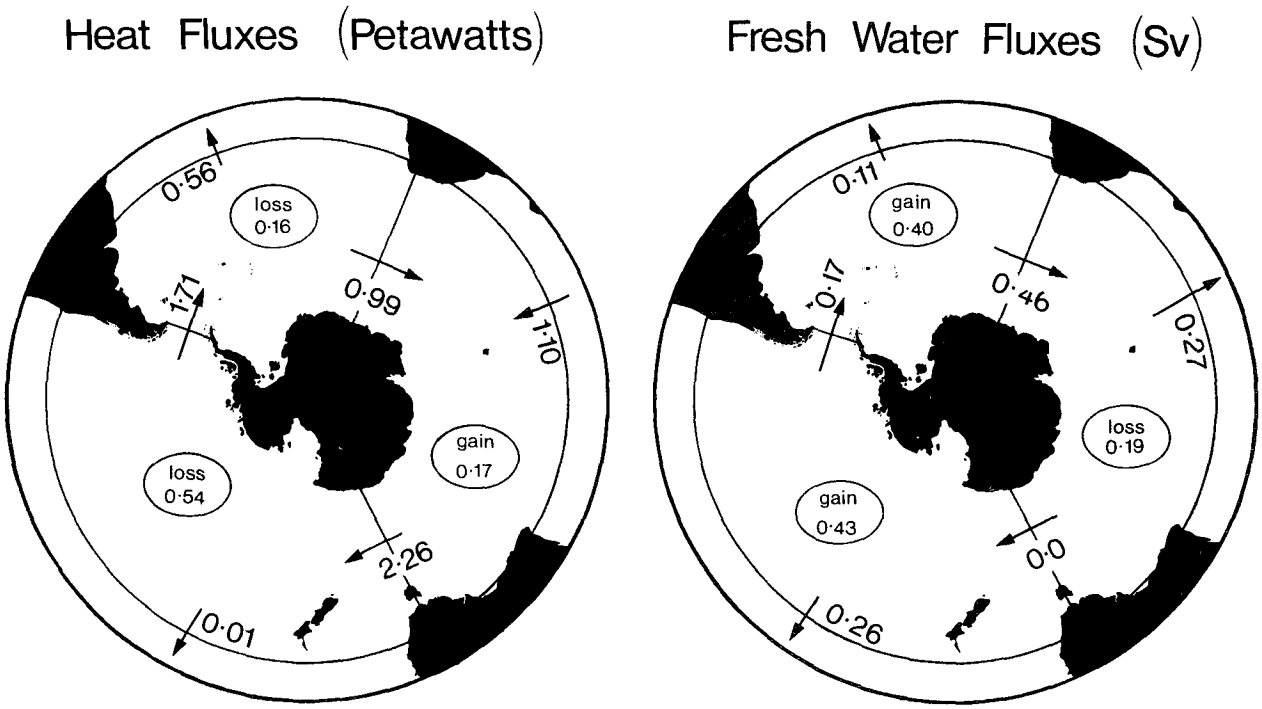


FIG. 8. Heat fluxes in petawatts (left) and freshwater fluxes in Sv (right) in the FRAM 6-year dataset. Their divergences are circled: loss implies loss from the ocean to the atmosphere and gain implies oceanic gain.

## 10. Conclusions

The authors are impressed by the success of FRAM in producing credible circulation and flux determinations given realistic annual wind forcing and ocean climatology. We believe that the project would have benefited if sensitivity studies had been undertaken. No attempt was made to vary the numerous parameters, some—but by no means all—of which are found in Table 1. It would then have been possible to address the question of the sensitivity of the six-year or equilibrium output to these variations.

The overall accuracy of the FRAM results is simply unknowable. First, as has been stated earlier, if a prognostic integration of FRAM to an equilibrium state were possible and a model climatology then constructed, the accuracy of a diagnostic integration could be assessed. Second, we have demonstrated that imperfections in the Levitus climatology, especially at great depth, introduce errors into the diagnostic integration. Since such integrations are likely to remain an important tool for investigating ocean circulation and fluxes, it is evident that we must seek improvements in defining the climatic state of the ocean. Thus, much work remains for both modelers and observationalists.

*Acknowledgments.* The paper owes its existence to the efforts of a small research group who developed and successfully implemented FRAM. We particularly acknowledge the input of Dr. D. Webb, who headed the project, offered helpful comments, and does not necessarily agree with all our conclusions.

## APPENDIX

Consider a zonal section in an ocean basin: $z$ is vertically upwards, $x$ is the zonal coordinate, and $v$ the meridional velocity.

The meridional transport in the basin is $T = \iint \rho v dx dz$ and the contribution to the transport from the geostrophic flow is $G = \iint \rho v_g dx dz$. Now

$$\rho v_g = \frac{1}{f}\frac{\partial p}{\partial x},$$

where $f$ is the Coriolis parameter, reckoned negative south of the equator. After substitution and integration we find:

$$G = \frac{1}{f}\int (p_A - p_B) dz,$$

where $p_A$ is the pressure on the left-hand margin and $p_B$ the value on the right. Note that $(p_A - p_B)\partial z$ is the horizontal pressure force needed to support the net geostrophic flow at depths $z$, $z + \partial z$ and acts on the ocean bottom.

If there is a zonal wind that exerts an $x$ component of the stress $\tau_x$, then there results an Ekman flow and an Ekman transport;

$$E = -\frac{1}{f}\int \tau_x dx.$$

Providing these contributions are the major ones to the transport, then

$$E + G \approx 0,$$

where we have invoked the important constraint that the total meridional transport is approximately zero.

Evidently, the horizontal force on the surface $\int \tau_x dx$ is opposed by a horizontal force on the bottom $-\int (p_A - p_B)dz$ and equality is assured by mass conservation. This result, we suppose, must have been known previously and we do not claim more than a rediscovery.

The result holds even in those latitudes of the Southern Ocean where in the upper 2000 m of the water column there is no topography. There is no net pressure force, nor any mean meridional geostrophic velocity. Below 2000 m there are net pressure forces on the bottom, which permit southward geostrophic flows to balance the shallow northward Ekman flow (Fig. 2) and yield a balance of force on the section.

## REFERENCES


Bryan, F., 1987: Parameter sensitivity of primitive equation ocean general circulation model. *J. Phys. Oceanogr.*, **17**, 970–985.

——, and Oort, A. H., 1984: Seasonal variation of the global water balance based on aerological data. *J. Geophys. Res.*, **89**, 11 717–11 730.

Bryden, H. L., 1979: Poleward heat flux and conversions of available potential energy in Drake Passage. *J. Mar. Res.*, **37**, 1–22.

——, and Hall, M. H., 1980: Heat transport by currents across 25°N latitude in the Atlantic Ocean. *Science*, **207**, 884–886.

Carissimo, B., A. H. Oort, and T. H. Vonder Haar, 1985: On estimating the meridional energy transports in the atmosphere and oceans. *J. Phys. Oceanogr.*, **15**, 82–91.

Chelton, D. B., A. M. Mestas-Nunez, and M. H. Freilich, 1990: Global wind stress and Sverdrup circulation from the Seasat scatterometer. *J. Phys. Oceanogr.*, **20**(8), 1175–1205.

Cox, M. D., 1984: A primitive equation, 3-dimensional model of the ocean. *Geophys. Fluid Dynamics Lab. Ocean Group Tech. Report*, No. 1. NOAA, 42 pp.

De Cuevas, B. A., 1990: FRAM—The Fine Resolution Antarctic Model. WOCE Newsletter, Institute of Oceanographic Sciences Deacon Laboratory, Wormley, England, **10**, p. 13.

De Szoeke, R. A., and M. D. Levine, 1981: The advective flux of heat by mean geostrophic motions in the Southern Ocean. *Deep-Sea Res.*, **28A**, 1057–1085.

Fuglister, F. C., 1960: Atlantic Ocean atlas of temperature and salinity profiles and data from the International Geophysical Year of 1957–1958. Woods Hole Oceanographic Institution Atlas Series, **1**, 209 pp.

Gill, A. E., 1973: Circulation and bottom water production in the Weddell Sea. *Deep-Sea Res.*, **20**, 111–140.

Hellerman, S., and M. Rosenstein, 1983: Normal monthly wind stress over the world ocean with error estimates. *J. Phys. Oceanogr.*, **13**, 1093–1104.

Hogg, N., P. Biscaye, W. Gardner, and W. J. Schmitz, Jr., 1982: On the transport and modification of Antarctic Bottom Water in the Vema Channel. *J. Mar. Res.*, (supplement) **40**, 231–263.

Holland, W. R., 1973: Baroclinic and topographic influences on the transport in western boundary currents. *Geophys. Fluid Dyn.*, **4**, 187–210.

Johnson, G. C., and H. L. Bryden, 1989: On the size of the Antarctic Circumpolar Current. *Deep-Sea Res.*, **36**, 39–53.

Killworth, P. D., 1987: Topographic instabilities in level model OGCMs. *Ocean Modelling*, **75**, 9–12.

Levitus, S., 1982: Climatological Atlas of the World Ocean. NOAA Professional Paper Number 13. U.S. Govt. Printing Office, Washington, D.C., 173 pp.

Peterson, R. G., and T. Whitworth, 1989: The subantarctic and polar fronts in relation to deep water masses through the southwestern Atlantic. *J. Geophys. Res.*, **94**(C8), 10 817–10 838.

Rintoul, S. R., 1988: Mass, heat and nutrient fluxes in the Atlantic Ocean determined by inverse methods. PhD. thesis, Massachusetts Institute of Technology and Woods Hole Oceanographic Institution, 287 pp.

Sarmiento, J. L., and K. Bryan, 1982: An ocean transport model for the North Atlantic. *J. Geophys. Res.*, **87**, 394–408.

Stevens, D. P., 1990: On open boundary conditions for three dimensional primitive equation ocean circulation models. *Geophys. and Astrophys. Fluid Dyn.*, **51**, 103–133.

——, 1992: The zonal momentum balance in a realistic eddy resolving general circulation model of the Southern Ocean. (In preparation)

Stommel, H., 1957: A survey of ocean current theory. *Deep-Sea Res.*, **4**, 149–184.

——, 1980: Asymmetry of interoceanic fresh-water and heat fluxes. *Proc. Natl. Acad. Sci. U.S.*, **77**, 2377–2381.

Toole, J. M., and M. E. Raymer, 1985: Heat and fresh water budgets of the Indian Ocean—revisited. *Deep-Sea Res.*, **32**, 917–928.

Warren, B. A., 1973: Transpacific hydrographic sections at Lats. 43°S and 28°S: The *Scorpio* Expedition—II. Deep water. *Deep-Sea Res.*, **20**, 9–38.

——, 1981: Transindian hydrographic section at Lat 18°S: property distributions and circulation in the South Indian Ocean. *Deep-Sea Res.*, **28**, 759–788.

Webb, D. J., et al. (The FRAM Group), 1991a: Using an eddy resolving model to study the Southern Ocean. *Eos*, **72**, 15 pp. 169, 174, 175.

——, et al., 1991b: The FRAM Atlas of the Southern Ocean, Natural Environment Research Council, 67 pp.

Whitworth, T., W. D. Nowlin, and S. J. Worley, 1982: The net transport of the Antarctic Circumpolar Current through Drake Passage. *J. Phys. Oceanogr.*, **12**, 960–971.

Woods, J. D., 1985: The World Ocean Circulation Experiment. *Nature*, **314**, 501–511.

World Ocean Circulation Experiment Implementation Plan 1988: Vol 1 and 2, World Climate Research Programme-11 and 12, World Meteorological Organization, Geneva.

Wunsch, C., D. Hu, and B. Grant, 1983: Mass, heat, salt and nutrient fluxes in the South Pacific Ocean. *J. Phys. Oceanogr.*, **13**, 725–753.